Supplement of Solid Earth, 16, 593–618, 2025
https://doi.org/10.5194/se-16-593-2025-supplement

Solid Earth
Open Access

Supplement of

Importance of forearc topography for the triggering of aftershocks of megathrust earthquakes: insights from mechanical models and the Tohoku-Oki and Maule earthquakes

Armin Dielforder et al.

Correspondence to: Armin Dielforder (armin.dielforder@uni-greifswald.de)

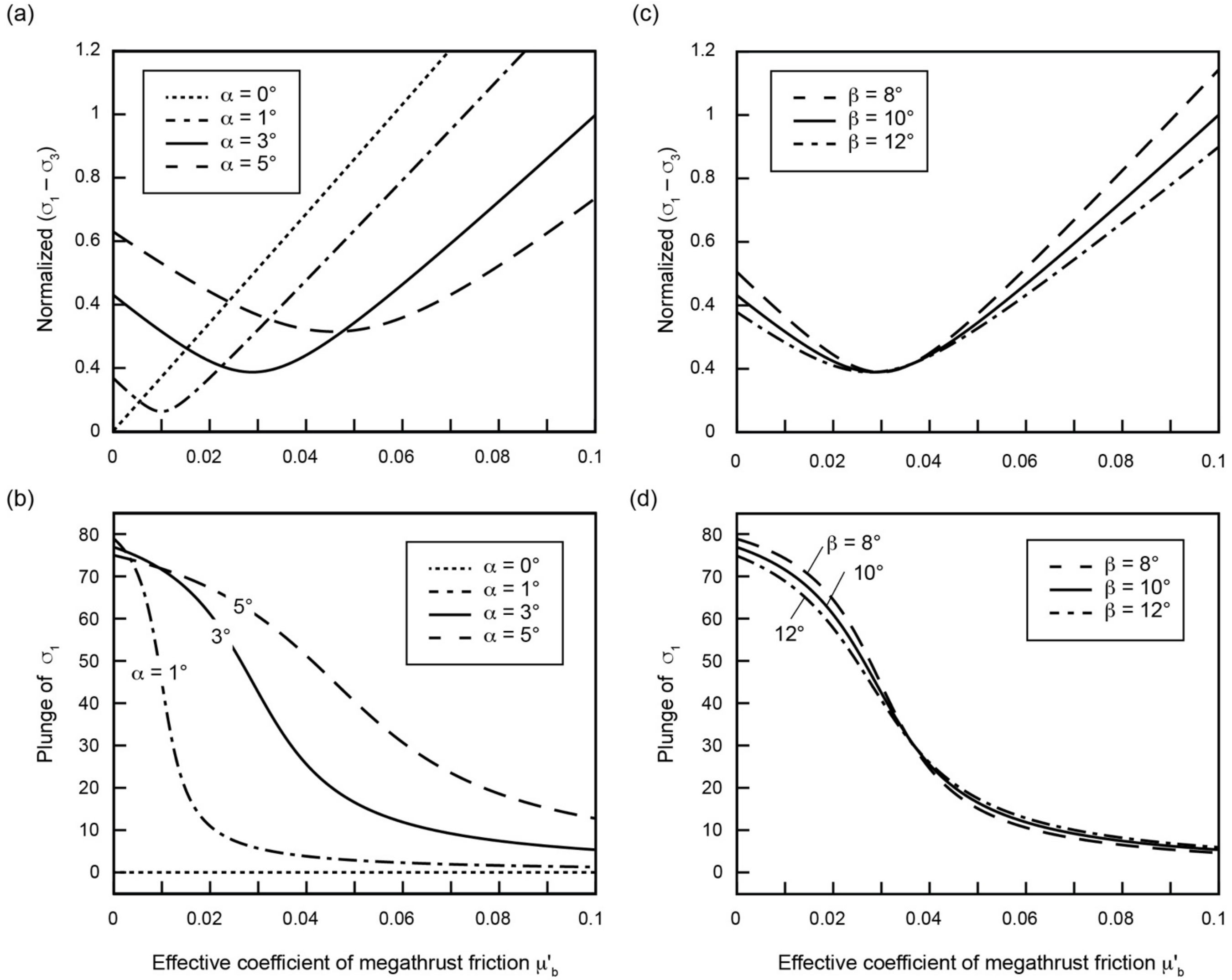

Figure S1: Analytical stress solutions for a stable dynamic Coulomb wedge. (a, b) Differential stress ($\sigma_1 - \sigma_3$) and plunge of σ_1 as function of μ'_b and for different surface slope angles α. (b, c) As (a) but for different basal dip angles β. Differential stress values are normalized to the maximum differential stress in the reference model (solid black lines for a = 3°, b = 10°).

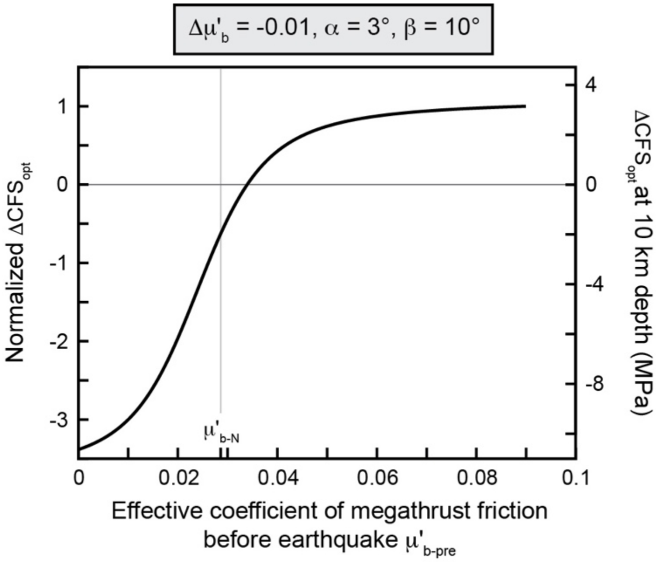

Figure S2: Coulomb failure stress change between optimal failure planes before and after the earthquake (ΔCFS_{opt}) for a negative megathrust stress drop and for coefficient of friction $\mu = 0.7$. The stress drop is given in terms of the change in effective coefficient of megathrust friction $\Delta\mu'_b$, with $\Delta\mu'_b = -0.01$. Solutions for the reference wedge model discussed in the main text. Left ordinate shows the Coulomb failure stress change normalized to the maximum value of ΔCFS_{opt}. Right ordinate indicates the Coulomb failure stress change at 10 km depth.

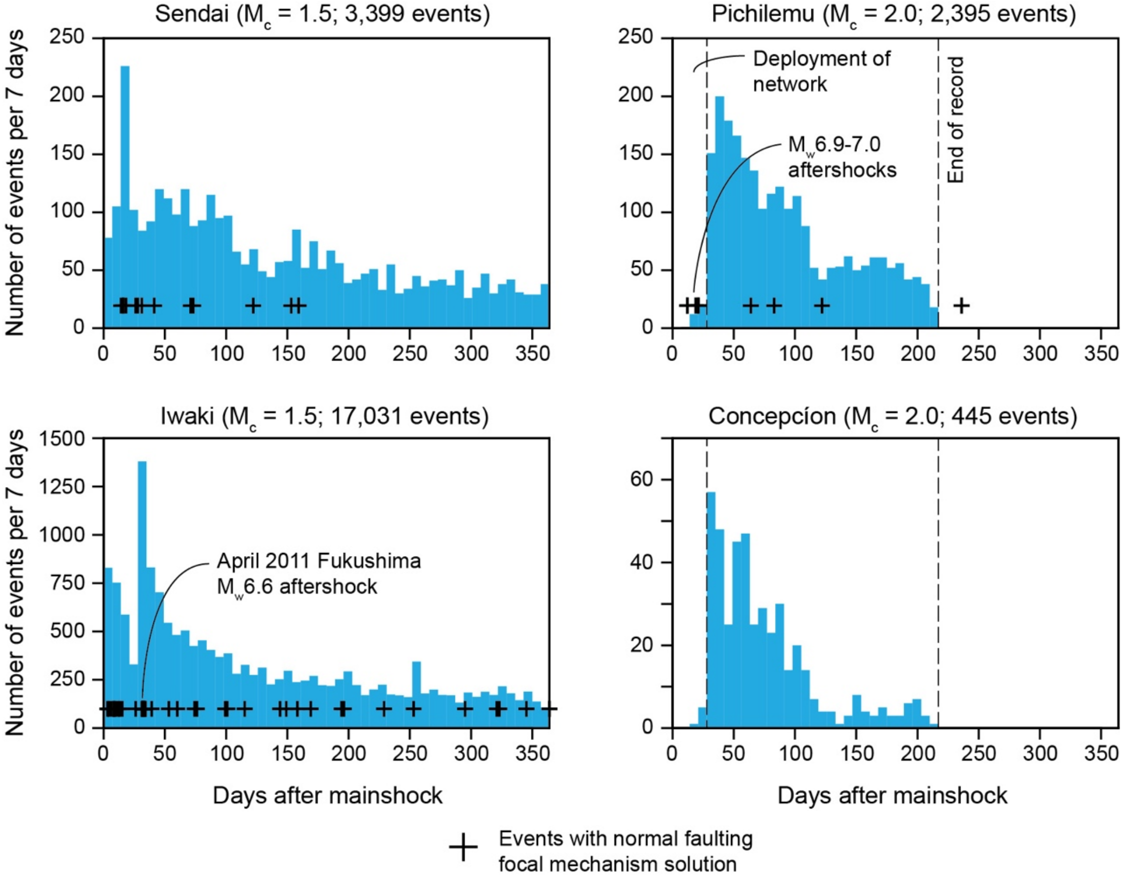

Figure S3: Number of earthquakes along the Sendai and Iwaki cross sections, Japan, and along the Pichilemu and Concepcíon cross sections, Chile, as function of days after mainshock (11 March 2011 for the Tohoku-Oki earthquake, Japan, and 27 February 2010 for the Maule earthquake, Chile). See Figs. 5a and 6a for location of cross sections. Black crosses indicate earthquakes with normal-faulting focal mechanism solutions. M_c is magnitude of completeness. Note that the detailed record for the Maule earthquake starts about 15 days after the mainshock and ends after 215 days. Data for the Sendai and Iwaki cross sections is from the Japan Meteorological Agency and for the Pichilemu and Concepcíon cross sections from Şen et al. (2015) and Lange et al. (2012).

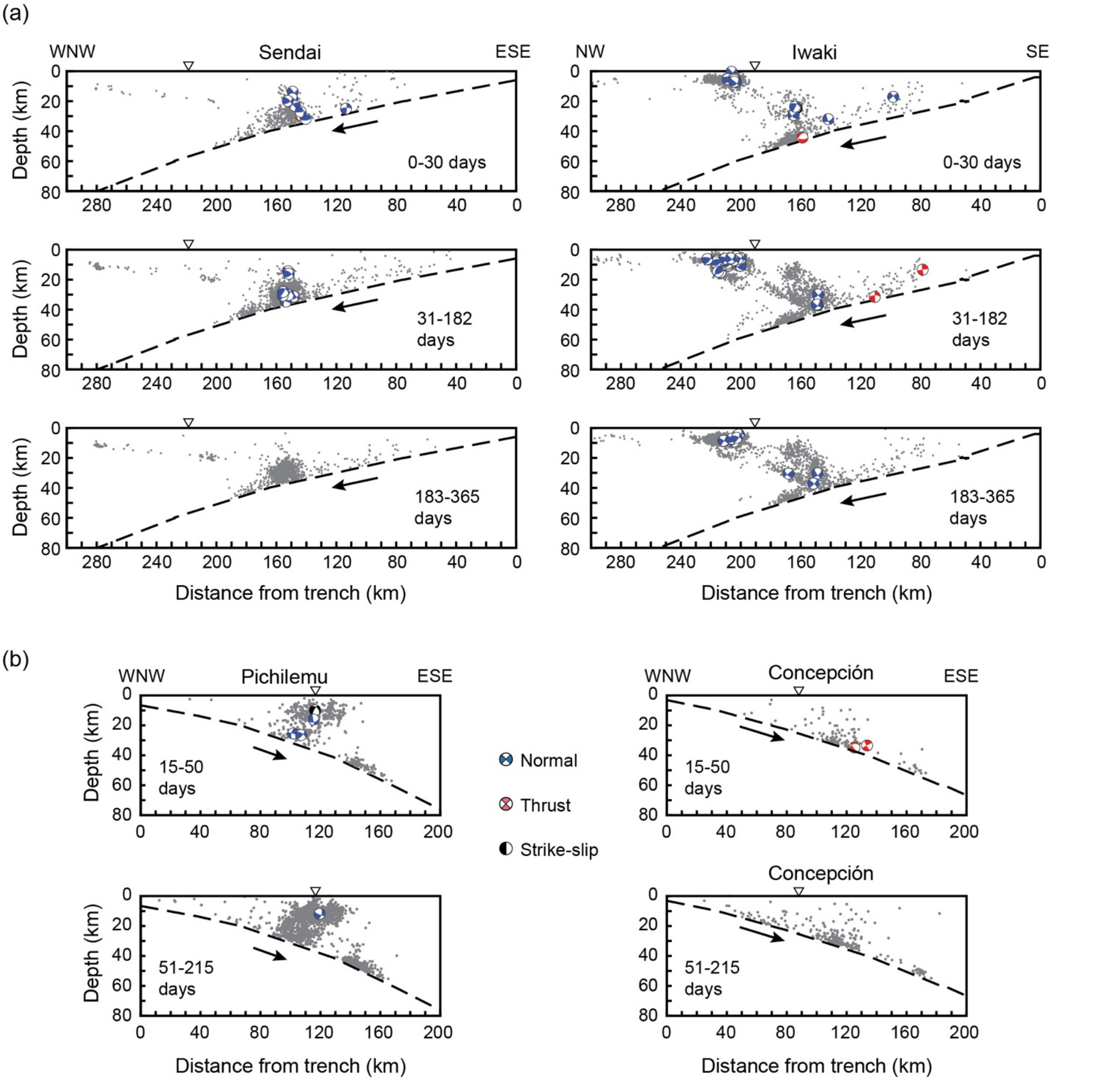

Figure S4: (a) Seismicity along the Sendai and Iwaki cross sections, Japan, for three different time periods after the 11 March 2011 Tohoku-Oki earthquake. (b) Seismicity along the Pichilemu and Concepcíon cross sections, Chile, for two different time periods after the 27 February 2010 Maule earthquake. Data for the Sendai and Iwaki cross sections is from the Japan Meteorological Agency and for the Pichilemu and Concepcíon cross sections from Şen et al. (2015) and Lange et al. (2012).

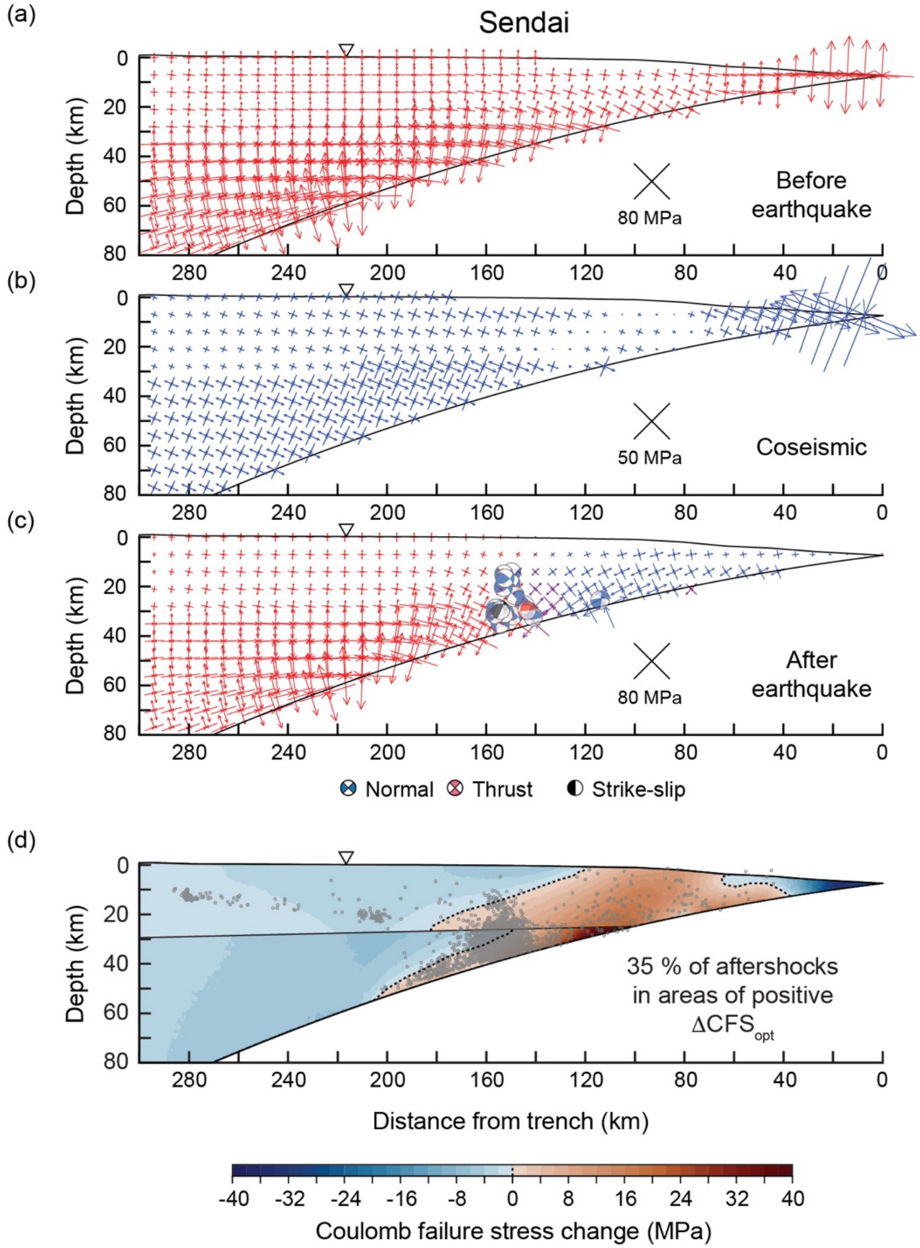

Figure S5: Supplementary model of forearc stress change for the Sendai cross section. See Fig. 5a for the location of the cross section. The model uses effective coefficients of megathrust friction that are increased by 0.01 relative to the main model presented in Fig. 7. Red and blue stress crosses in (a-c) indicate that the plunge of σ_1 is less than 40° (deviatoric compression) and more than 50° (deviatoric tension), respectively; purple crosses indicate a plunge of σ_1 between 40° and 50°. The size of the stress crosses scale with the differential stress. (a) Deviatoric stress before the earthquake. (b) Incremental change in deviatoric stress caused by the earthquake. (c) Deviatoric stress after the earthquake. Beach balls indicate focal mechanism solutions of aftershocks (cf. Fig. 5). (d) Coseismic change in Coulomb failure stress calculated for $\mu = 0.7$.

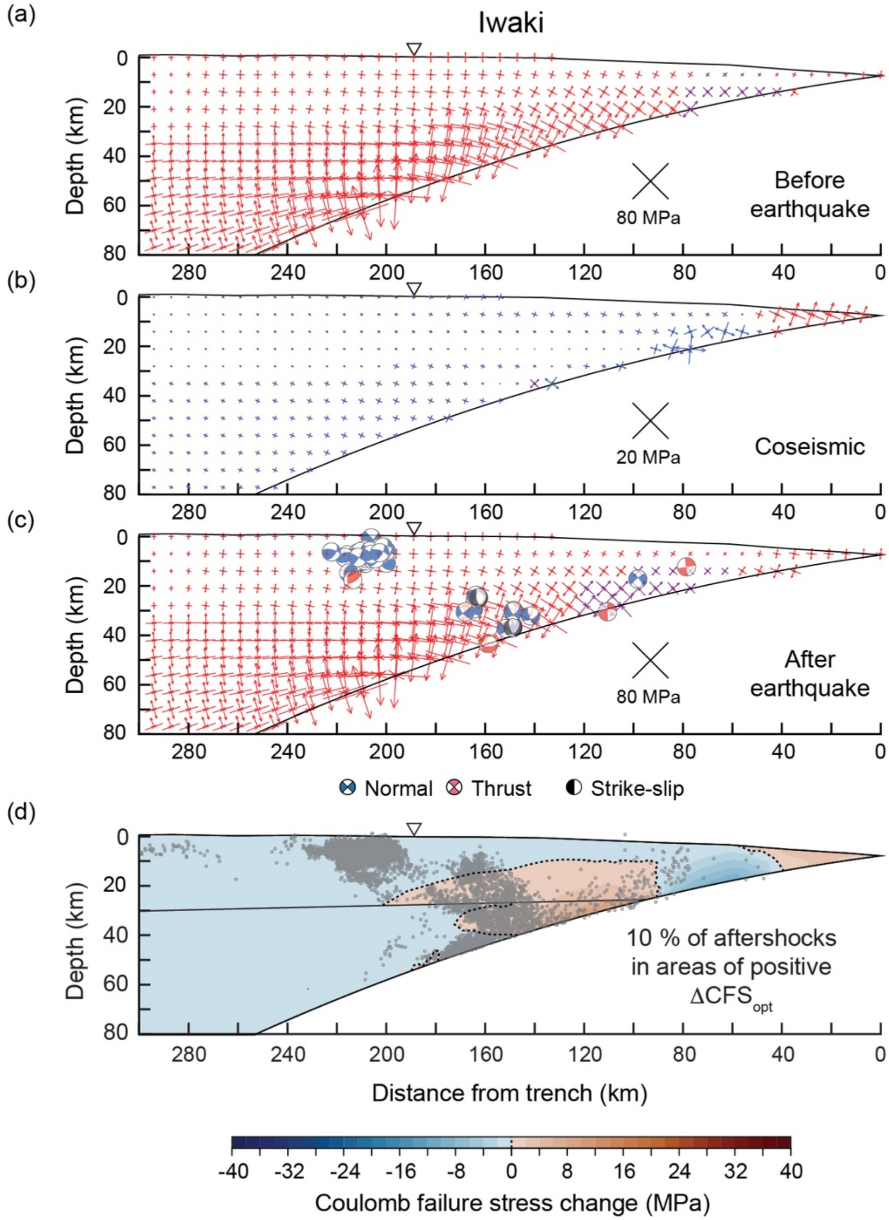

55 **Figure S6: Supplementary model of forearc stress change for the Iwaki cross section. See Fig. 5a for the location of the cross section. The model uses effective coefficients of megathrust friction that are increased by 0.01 relative to the main model presented in Fig. 8. The meaning of panels (a-d) is the same as in Fig. S5. Coseismic change in Coulomb failure stress calculated for $\mu = 0.7$.**

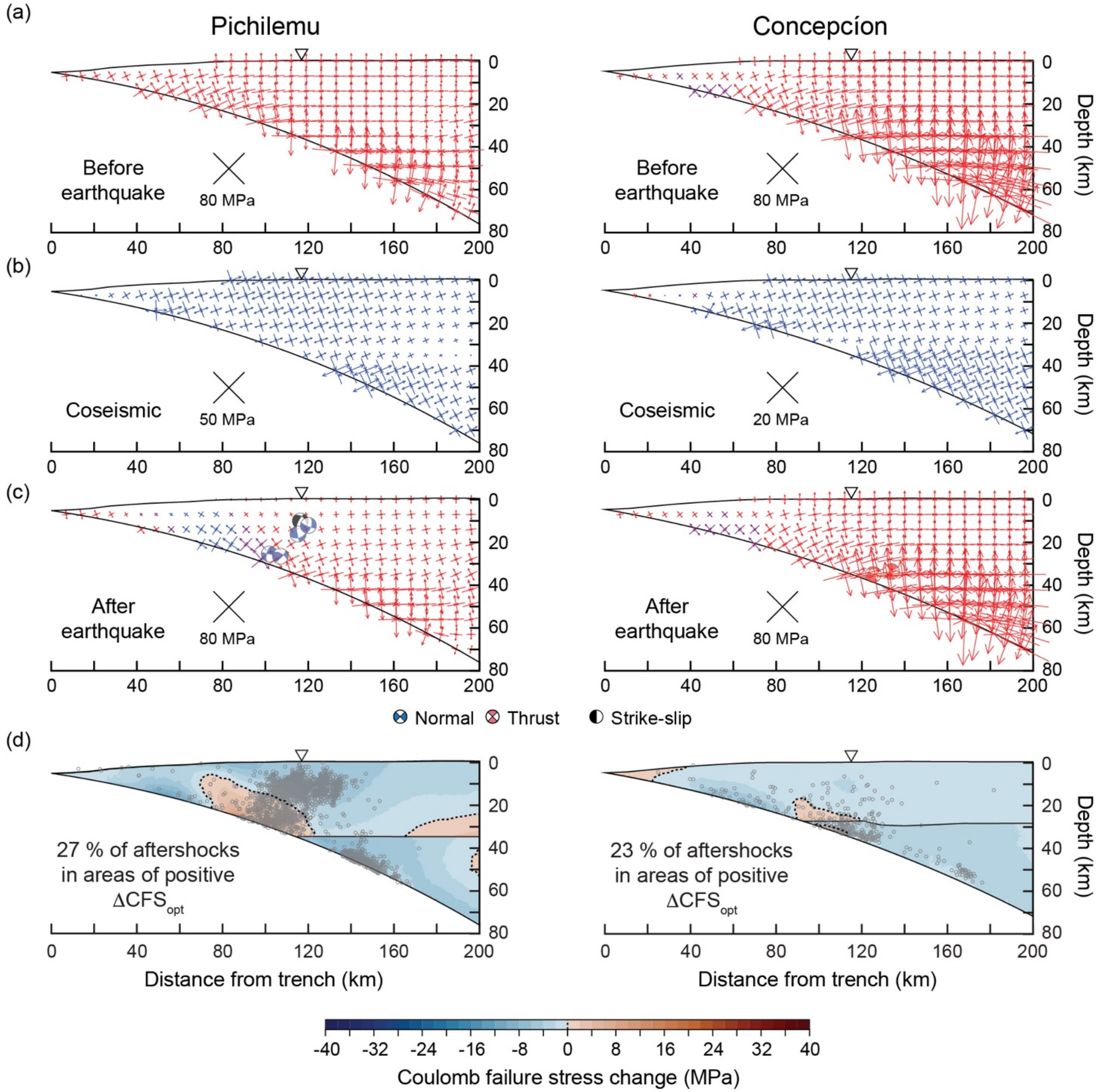

Figure S7: Supplementary models of forearc stress change for the Pichilemu and Concepcíon cross sections. See Fig. 6a for the location of the cross sections. The models use effective coefficients of megathrust friction that are increased by 0.01 relative to the main model presented in Fig. 9. The meaning of panels (a-d) is the same as in Fig. S5. Coseismic change in Coulomb failure stress calculated for $\mu = 0.7$.

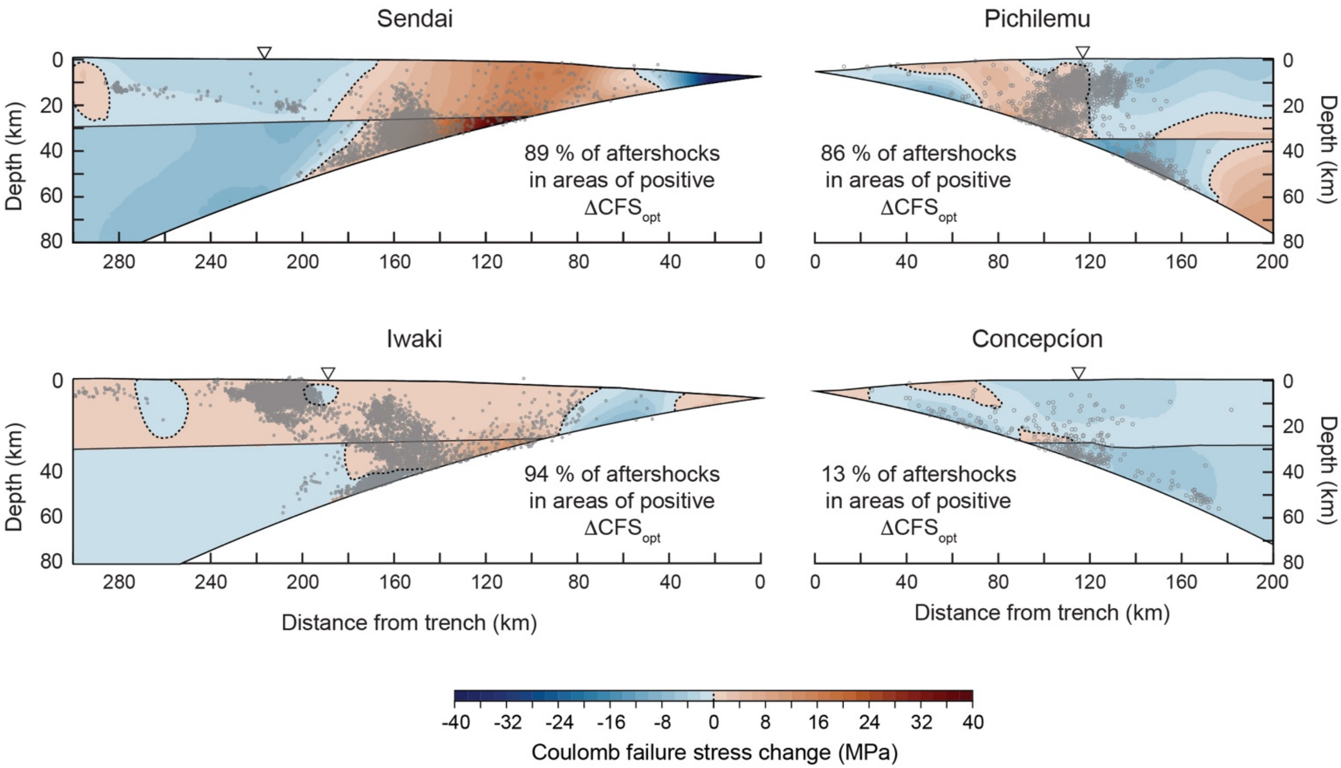

65

Figure S8: Supplementary Coulomb failure stress models using a coefficient of friction of μ = 0.2. Total stresses and megathrust stress drop are the same as in Figs. 7-9.

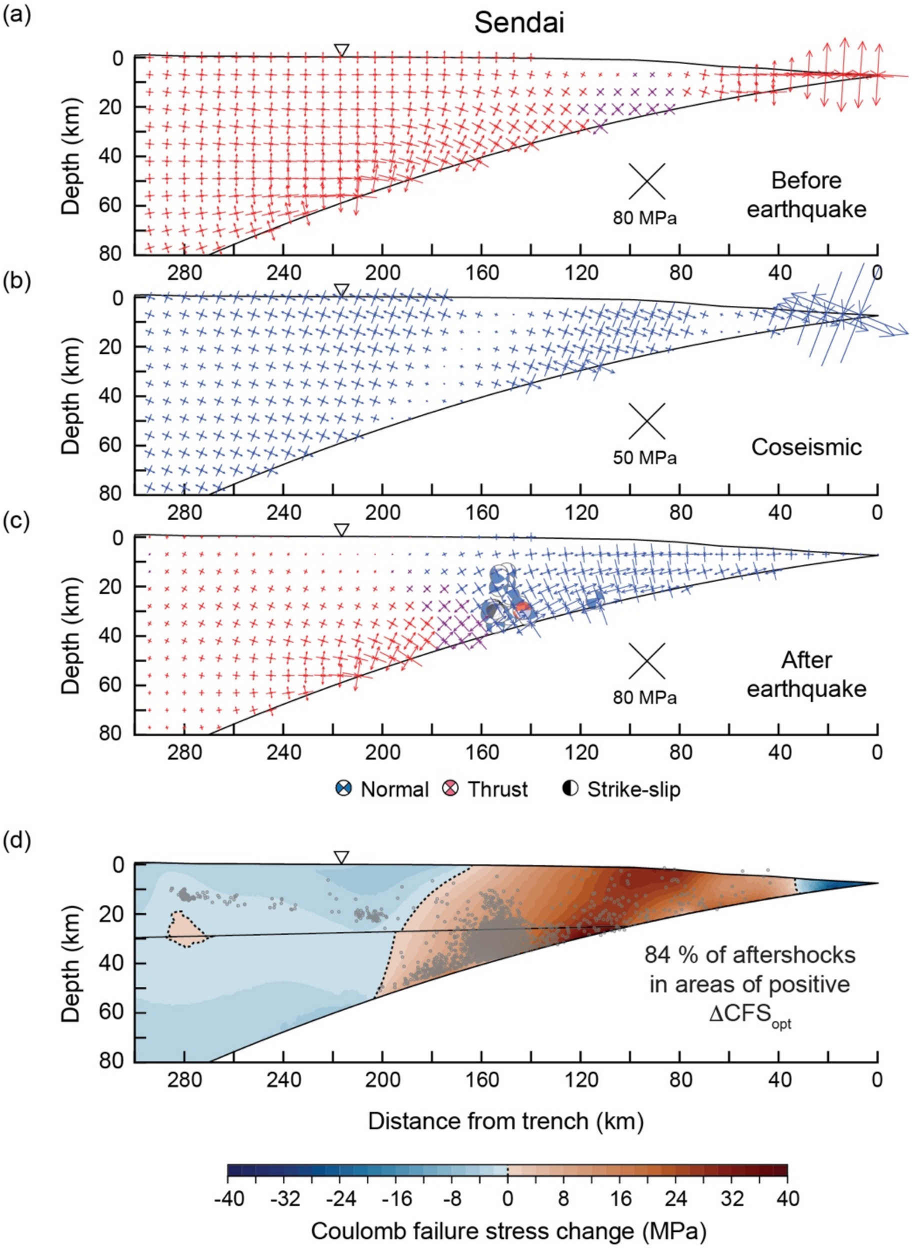

70 **Figure S9: Supplementary model of forearc stress change for the Sendai cross section. See Fig. 5a for the location of the cross section. The model uses the same Young's modulus of 60 GPa for the crust and mantle. The meaning of panels (a-d) is the same as in Fig. S5. Coseismic change in Coulomb failure stress calculated for μ = 0.7.**

75

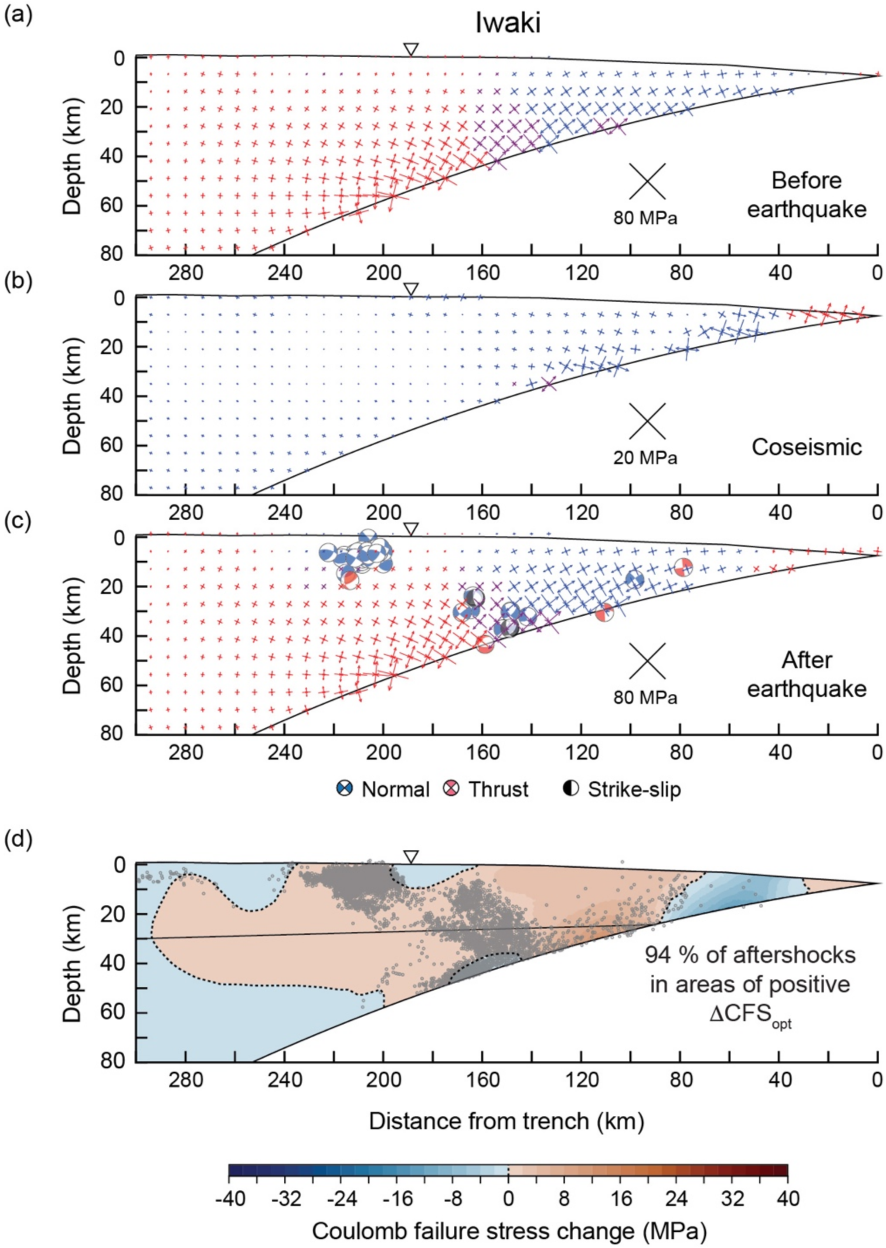

Figure S10: Supplementary model of forearc stress change for the Iwaki cross section. See Fig. 5a for the location of the cross section. The model uses the same Young's modulus of 60 GPa for the crust and mantle. The meaning of panels (a-d) is the same as in Fig. S5. Coseismic change in Coulomb failure stress calculated for μ = 0.7.

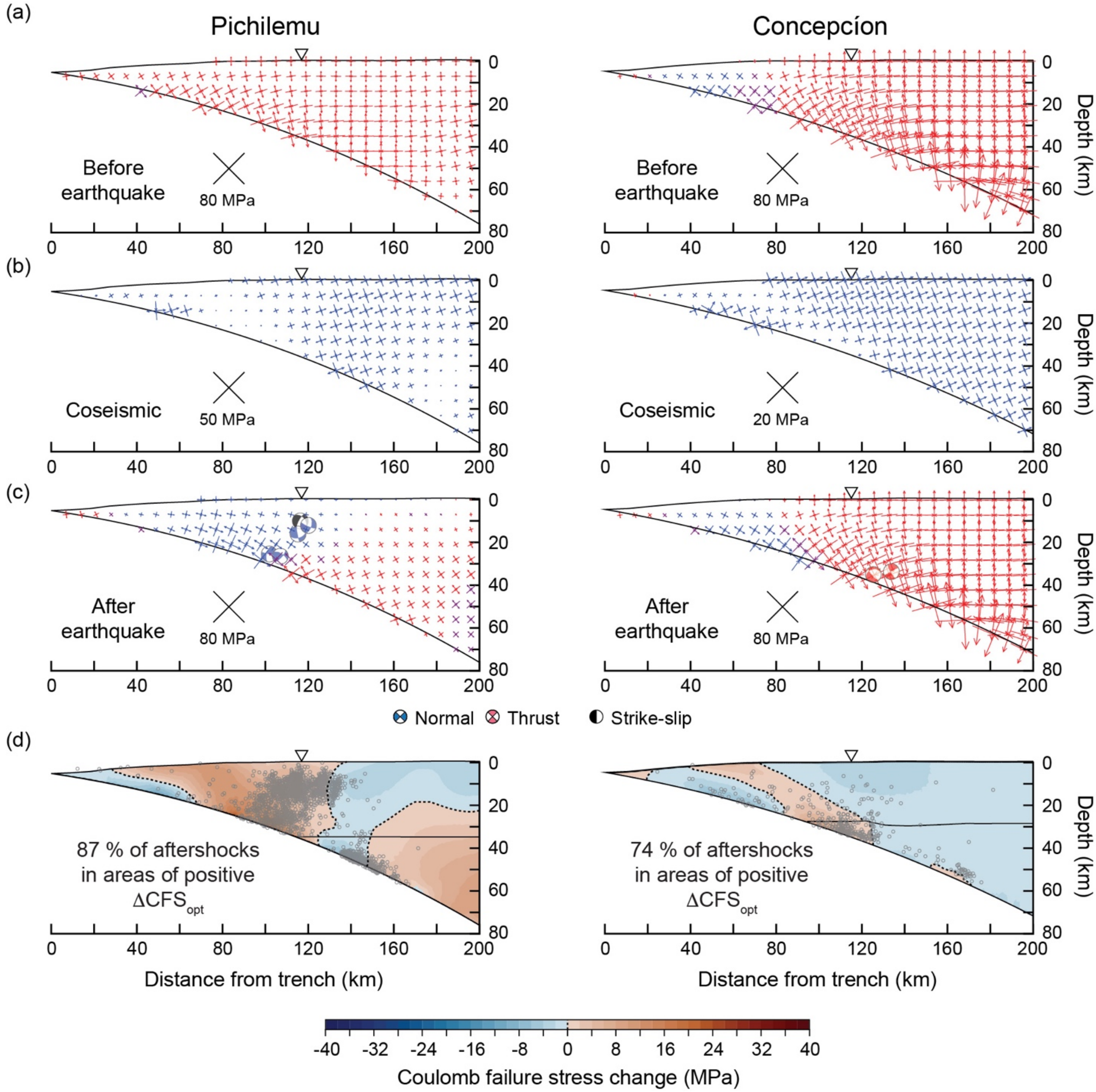

Figure S11: Supplementary models of forearc stress change for the Pichilemu and Concepcíon cross sections. See Fig. 6a for the location of the cross section. The model uses the same Young's modulus of 60 GPa for the crust and mantle. The meaning of panels (a-d) is the same as in Fig. S5. Coseismic change in Coulomb failure stress calculated for $\mu = 0.7$.

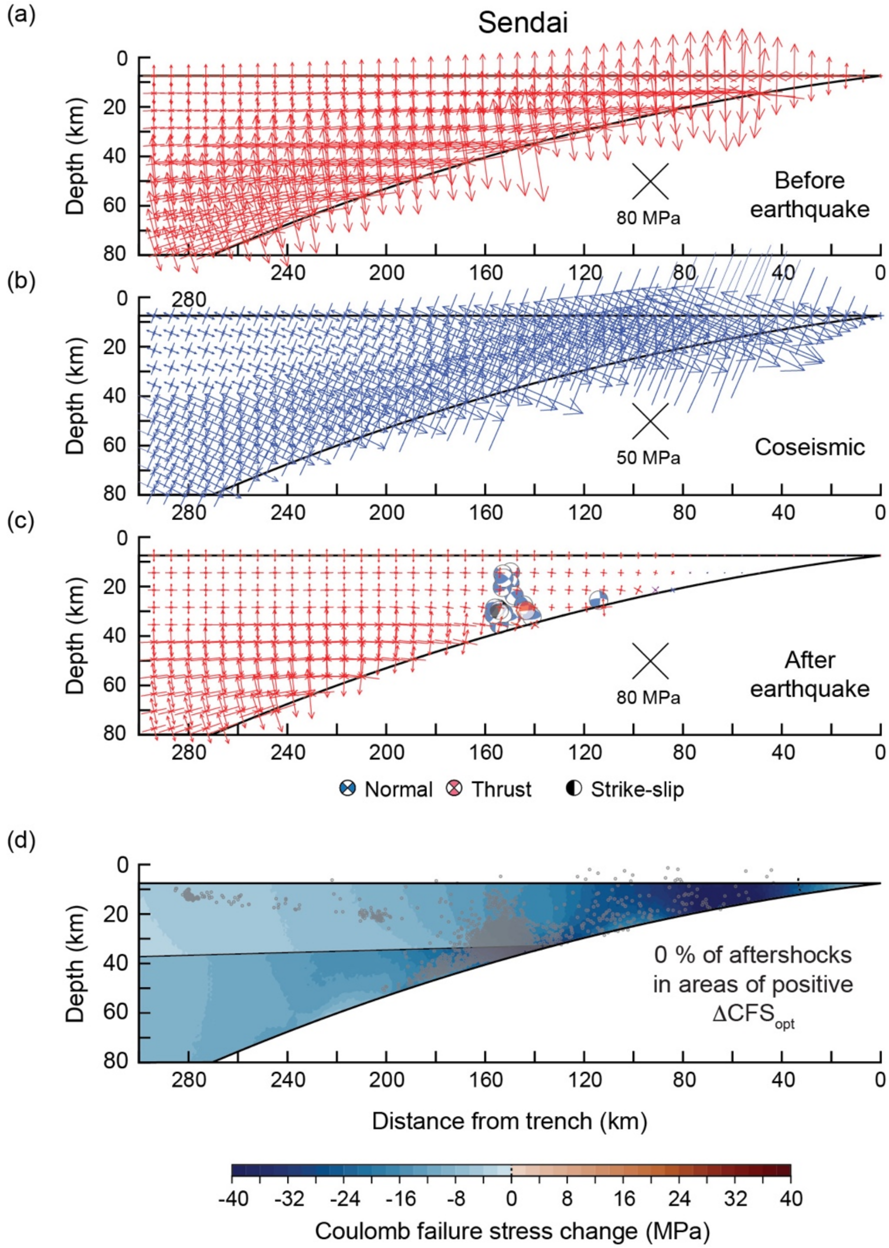

Figure S12: Supplementary model of forearc stress change for the Sendai cross section. See Fig. 5a for the location of the cross section. The forearc has a flat surface and water loads have been removed such that there are no gradients in potential energy (no topographic stresses). The surface is located at the original trench depth, to maintain the depth and length of the plate interface as in the model with topography. The meaning of panels (a-d) is the same as in Fig. S5. Coseismic change in Coulomb failure stress calculated for $\mu = 0.7$.

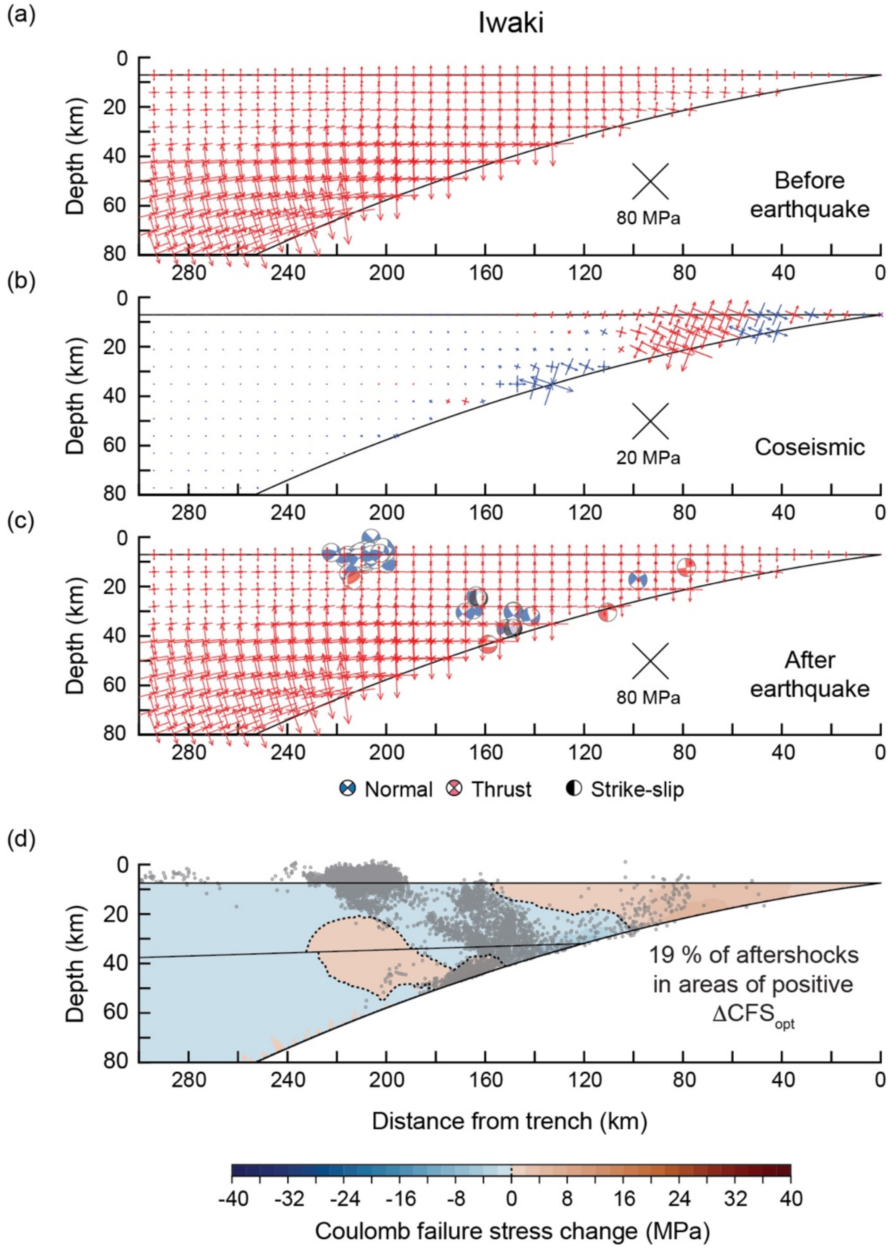

Figure S13: Supplementary model of forearc stress change for the Iwaki cross section. See Fig. 5a for the location of the cross section. The forearc has a flat surface and water loads have been removed such that there are no gradients in potential energy (no topographic stresses). The surface is located at the original trench depth, to maintain the depth and length of the plate interface as in the model with topography. The meaning of panels (a-d) is the same as in Fig. S5. Coseismic change in Coulomb failure stress calculated for $\mu = 0.7$.

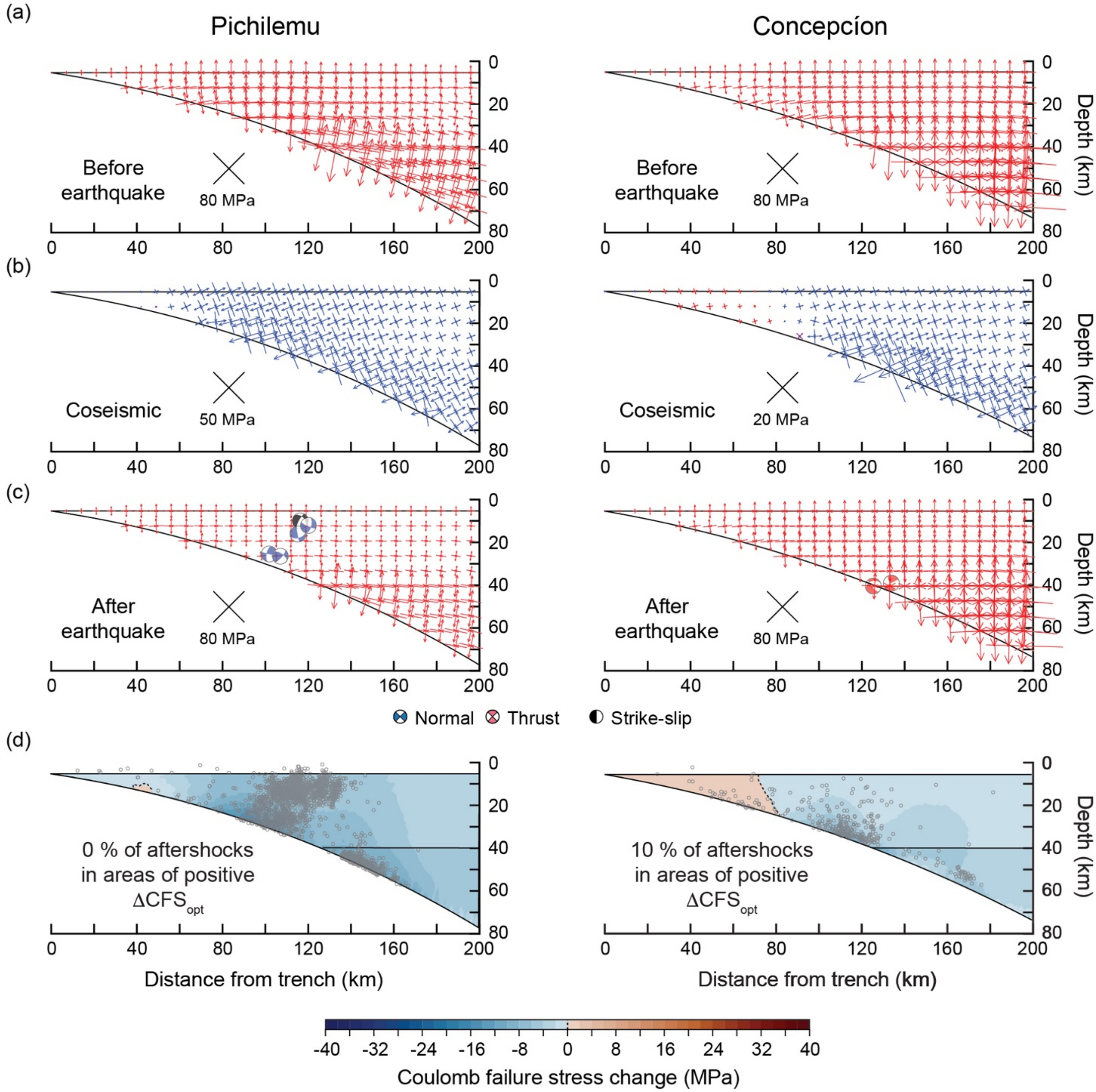

Figure S14: Supplementary models of forearc stress change for the Pichilemu and Concepcíon cross sections. See Fig. 6a for the location of the cross section. In both cross sections, the forearc has a flat surface and water loads have been removed such that there are no gradients in potential energy (no topographic stresses). The surface is located at the original trench depth, to maintain the depth and length of the plate interface as in the model with topography. The meaning of panels (a-d) is the same as in Fig. S5. Coseismic change in Coulomb failure stress calculated for $\mu = 0.7$.